Simulation of debris flows in the Central Andes based on Open Source GIS: possibilities, limitations, and parameter sensitivity

Martin Mergili, Wolfgang Fellin, Stella M. Moreiras & Johann Stötter

Natural Hazards
Journal of the International Society for the Prevention and Mitigation of Natural Hazards

ISSN 0921-030X
Volume 61
Number 3

Nat Hazards (2012) 61:1051-1081
DOI 10.1007/s11069-011-9965-7

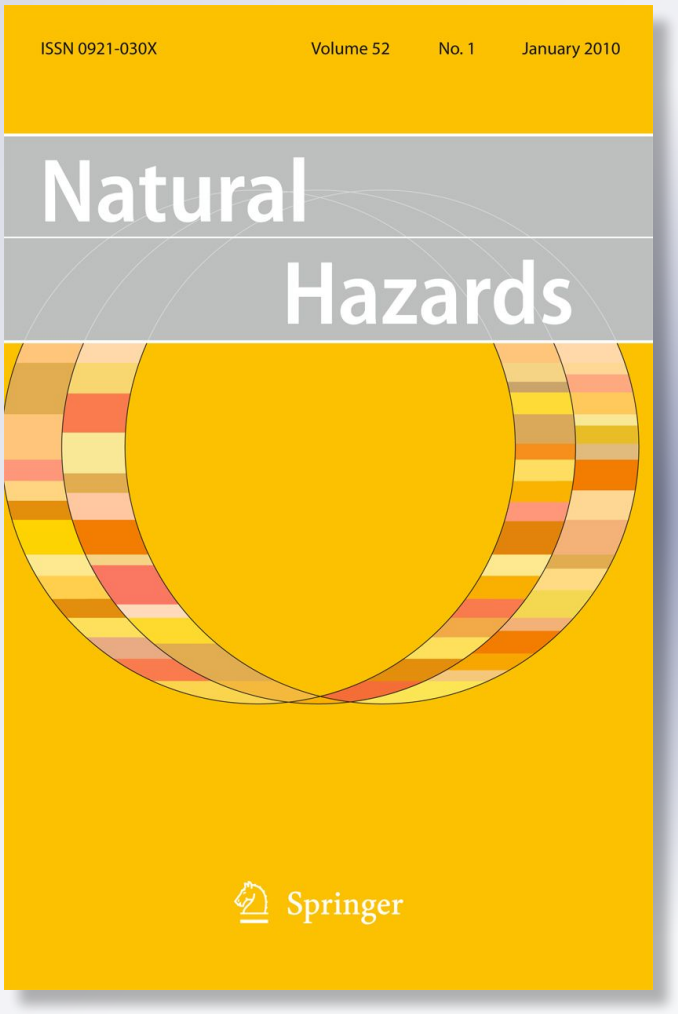

Springer

Nat Hazards (2012) 61:1051–1081
DOI 10.1007/s11069-011-9965-7

ORIGINAL PAPER

Simulation of debris flows in the Central Andes based on Open Source GIS: possibilities, limitations, and parameter sensitivity

Martin Mergili · Wolfgang Fellin · Stella M. Moreiras · Johann Stötter

Received: 4 March 2009 / Accepted: 22 August 2011 / Published online: 7 September 2011

Abstract A GIS-based model framework, designed as a raster module for the Open Source software GRASS, was developed for simulating the mobilization and motion of debris flows triggered by rainfall. Designed for study areas up to few square kilometres, the tool combines deterministic and empirical model components for infiltration and surface runoff, detachment and sediment transport, slope stability, debris flow mobilization, and travel distance and deposition. The model framework was applied to selected study areas along the international road from Mendoza (Argentina) to Central Chile. The input parameters were investigated at the local scale. The model was run for a number of rainfall scenarios and evaluated using field observations and historical archives in combination with meteorological data. The sensitivity of the model to a set of key parameters was tested. The major scope of the paper is to highlight the capabilities of the model—and of this type of models in general—as well as its limitations and possible solutions.

Keywords Debris flows · GIS · Simulation · Central Andes · Parameter sensitivity

M. Mergili (✉)
Institute of Applied Geology, BOKU University Vienna, Peter Jordan Straße 70, 1190 Vienna, Austria
e-mail: martin.mergili@boku.ac.at

W. Fellin
Division of Geotechnical and Tunnel Engineering, Department of Infrastructure,
University of Innsbruck, Technikerstraße 13, 6020 Innsbruck, Austria

S. M. Moreiras
Instituto Argentino de Nivología, Glaciología y Ciencias Ambientales (IANIGLA),
Avenida Ruíz Leal s/n Parque General San Martín, CP5500 Mendoza, Argentina

J. Stötter
Institute of Geography, University of Innsbruck, Innrain 52, 6020 Innsbruck, Austria

1 Introduction

Debris flows are rapid mass movements of water and debris representing a considerable hazard when interfering with people, buildings, or infrastructures. They are often triggered by heavy or prolonged rainfall or by extreme snow melt. Mobilization of debris flow material often occurs due to translational or rotational failure of saturated or undercut slopes or due to entrainment of regolith by surface runoff or by the debris flow itself. Various models exist for simulating the involved sub-processes, e.g. particle entrainment, regolith hydrology, slope stability, or debris flow motion. More integrated GIS-based approaches as attempted for example by Burton and Bathurst (1998) or by Wichmann (2006) are extremely valuable for a quick assessment of debris flow hazard as a response to defined meteorological and hydrological conditions. The present paper describes a method for integrated modelling of debris flows (from triggering to deposition) based on the software GRASS GIS. As an Open Source GIS package with focus on raster processing, GRASS facilitates model development, distribution, and evaluation: the program code is freely accessible and new modules may be added by anybody. Therefore, the entire scientific community has the chance to contribute to the evaluation of the model and the further development of the program code. The present paper focuses on the assessment of the potentials and limitations of the model—and of this type of models in general—and on its sensitivity to certain key input parameters. For this purpose, various combinations of parameter settings were evaluated using six small catchments in the Central Andes (Argentina and Chile).

2 Background

2.1 Debris flows: landslides or runoff?

At first glance, the term debris flow does not always refer to exactly the same process. Some authors rather consider it as landslide with a fluid-like motion (Burton and Bathurst 1998; Corominas et al. 2003; Moreiras 2004a, b), others consider it as runoff with very high sediment concentration (Rickenmann 1999; O'Brien 2003). However, these two approaches are not necessarily contradictory—they rather depend on whether the observer has a geotechnical or a hydrological background. As stated by Rickenmann (1999), debris flows are phenomena intermediate between landslides and runoff. Many debris flow events in the real world share features of both types of processes, but most of them have a clear tendency to the one or the other. Some authors distinguish between debris flows on slopes originating from landslides and debris flows in channels mobilized in or near to the stream bed (Wichmann 2006). Process chains coupling landslides, runoff, and debris flows are common.

2.2 Modelling of debris flows

Integrated simulation models for debris flows require the inclusion of model components for all relevant sub-processes, whereby the most important are slope stability, detachment by surface runoff (both of them including hydraulic triggers), and debris flow motion. The following review focuses on methods applicable in combination with Geographic Information Systems (GIS).

2.2.1 Slope stability

The basic concept of slope stability modelling is the factor of safety, or factor of stability, FOS, in its most simple formulation:

$$\mathrm{FOS} = \frac{\text{stabilizing forces}}{\text{destabilizing forces}}. \quad (1)$$

Values of FOS < 1 indicate unstable conditions. The so-called infinite slope stability model assumes a plane, infinite slope, and a plane slip surface parallel to the slope surface. These conditions are never met in reality but are a reasonable approximation for shallow slope failures. Strictly spoken, the infinite slope stability model works for cohesionless regolith only. Various authors have applied this method in combination with GIS, like Burton and Bathurst (1998) or Xie et al. (2004), or coupled to a probabilistic approach, i.e. SINMAP (Pack et al. 1998). The infinite slope stability model is often coupled to a hydraulic model: seepage forces on the one hand and the change of effective stress due to pore water pressure on the other hand play a prominent role when regarding slope stability (Wilkinson et al. 2002; Xie et al. 2004).

2.2.2 Detachment and sediment transport

Surface runoff exerts a flow shear stress τ (N m^{-2}) on the underlying regolith:

$$\tau = \rho g R S, \quad (2)$$

where ρ (kg m^{-3}) is the flow density, g (m s^{-2}) is the gravitational acceleration, R (m) is the hydraulic radius, and S (m m^{-1}) is the hydraulic energy gradient. Excess shear stress can be used for computing the detachment capacity D_c (kg m^{-2} s^{-1}) as follows (Knapen et al. 2007):

$$D_c = K_c(\tau - \tau_{cr})^b, \quad (3)$$

where K_c (kg^{1-b} s^{2b-1} m^{b-2}) is the concentrated flow regolith erodibility, τ_{cr} (Pa) is the critical shear stress, and b is an exponent. All these parameters have to be derived empirically. Analogous approaches exist for other flow variables, particularly stream power.

The sediment concentration of a flow decreases the flow's capability to detach more regolith, probably due to reduced turbulence (Knapen et al. 2007). Some approaches do exist to account for this effect, for example

$$D_r = D_c\left(1 - \frac{q_s}{T_c}\right), \quad (4)$$

where D_r (kg m^{-2} s^{-1}) is the detachment rate, q_s is the sediment load, and T_c is the transport capacity. If D_r is negative, deposition of the transported sediment starts.

Various authors have suggested predominantly or fully empirical sediment transport equations, for example Schoklitsch (1962), Yalin (1963), Yang (1973), Bagnold (1980), Low (1989), Govers (1990), Rickenmann (1990), or Abrahams et al. (2001). The Rickenmann (1990) equation—only including bedload—is best suited for relatively steep channels and high load (Hessel and Jetten 2007).

2.2.3 Debris flow motion

The motion of debris flows shows properties different from the flow of clear water, requiring specialized and complex methods to be modelled in a fully deterministic way

Table 1 Concepts for modelling the motion of debris flows

	Description	Potentials	References
Empirical–statistical	Regression functions, threshold values, or equivalent friction angles derived from large datasets of past events	Pre-assessment at regional scale	Vandre (1985), Rickenmann (1999), Corominas et al. (2003)
Semi-deterministic	Deterministic equations for flow parameters (velocity), assumption of mass points routed with random walk	Case studies at regional and local scale	Perla et al. (1980), Gamma (2000), Wichmann (2006)
Deterministic	Physically based approaches based on rheological assumptions	Detailed studies at the local scale, prediction of future events	Savage and Hutter (1989), Hungr (1995), Iverson (1997)

(Savage and Hutter 1989; Hungr 1995; Iverson 1997). Chau and Lo (2004) modified the model of Takahashi et al. (1992) in order to model flow path and deposition of debris flows threatening the Leung King Estate (Hong Kong, China), based on a GIS. Implementation of the Savage-Hutter theory into GIS is a challenge because of non-rectangular coordinate systems used (Mergili et al. 2008).

Due to these difficulties, more simple models—with due limitations—were developed, particularly in combination with GIS. Table 1 summarizes the three major categories of models for the motion and deposition of debris flow material.

3 Study areas

Six small catchments along the international Trans-Andean road corridor from Mendoza (West Central Argentina) to Central Chile were selected as study areas for the present paper (Fig. 1). The major geometric characteristics of all the study areas and estimated debris flow volumes are summarized in Table 2. Volumes include the estimated apparent quantity of regolith removed from the area by debris flow processes. The broad ranges of volumes are primarily related to uncertain depths.

Four study areas are located in the Mendoza valley separating the Precordillera and the Cordillera Frontal at a place called Guido, about 100 km W of Mendoza and 25 km SE of Uspallata. The climate is arid with a mean annual precipitation of 200 mm, occurring primarily as heavy rainstorms during summer. A large granitic body has produced systems of steep slopes of weathered material, making the area highly susceptible to debris flows (Fig. 2). Several events have been reported in the past (Moreiras 2004a, b, 2005). Quantitative data are available in terms of debris volume removed from the road (Espejo 1996; Table 3).

Two study areas are located on the Chilean side of the Cordillera Principal. Debris flow activity is well documented for both areas. Also here, the main source of quantitative data were reports specifying the debris volume removed from the international road (Hauser 2000a, b, 2005; see Table 3). *Quebrada del Ferrocarril* represents a system of gullies draining directly onto the road near to Portillo, frequently producing debris flows connected to rapid snow melt. Farther down, close to the village of *Guardia Vieja*, a mass of till has repeatedly shown aggressive responses to heavy or prolonged rainfall events, particularly during El Niño periods. The climate has a mediterranean character with a mean

Fig. 1 Study areas (*shaded relief map* derived from SRTM data provided by Jarvis et al. 2008)

Table 2 Geometric characteristics of the study areas and debris flow volumes

Area	A (km^2)	zmin (m)	zmax (m)	αavg (°)	V (1,000 m^3)
La Ampolleta	2.31	1,498	2,733	25.0	7–15
Quebrada Escondida	0.73	1,523	2,312	33.2	3–6
Castillo de Rocas	0.80	1,512	2,492	31.9	7–35
Guido—Las Murallas	0.71	1,507	2,304	35.6	10–50
Quebrada del Ferrocarril	1.66	2,333	4,009	34.5	20–75
Guardia Vieja	1.94	1,502	2,659	26.9	>140

A is the total surface area of the catchment, z_{min} and z_{max} are minimum and maximum elevation, α_{avg} is average slope angle, and *V* is debris flow volume

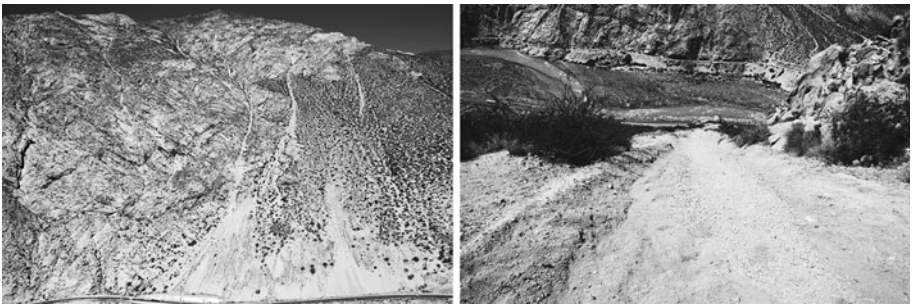

Fig. 2 Study area *Castillo de Rocas* with debris flow channel

annual precipitation of 500–600 mm. In the El Niño year 1987, almost 1,800 mm were recorded at the Río Blanco meteorological station. A period of 6 days with more than 450 mm precipitation triggered a flow of debris and mud blocking the international road (see Table 3).

Table 3 A selection of documented debris flows in the study areas

Date	Study area	Rainfall on day of event (mm)	5 days antecedent precipitation (mm)	Removed vol. (m^3)	Source
13.08.1987	Guardia Vieja	148.0	309.5	45,000	Hauser (2000b)
08.03.1996	Guido (all)	9.2	2.5	15,000[a]	Espejo (1996)
21.03.1996	Guido (all)	40.0	4.0	600[a]	Espejo (1996)
18.11.2000	Qd. Ferrocarril	Snow melt		10,000	Hauser (2005)
21.01.2003	Qd. Ferrocarril	Snow melt		8,000	Hauser (2005)
17.11.2004	Qd. Ferrocarril	Snow melt		14,000	Hauser (2005)

[a] Including material from rock fall

Table 4 Input data and parameters

Database	Data format	Use	Sources
Imagery	Spatial (raster)	Derivation of orthophotographs, elevation models, regolith class, and land cover maps	Regional, national, and international authorities; own images
Elevation and relief	Spatial (raster)	All model components	Stereo-matching of imagery
Regolith (physical, mechanical, and hydraulic parameters)	Spatial (classes) and tabular	Infiltration model, slope stability model	Mapping; sampling and laboratory analysis; literature values
Land cover and surface	Spatial (classes) and tabular	Hydraulic and slope stability model components	Mapping; literature values (see text for references)
Meteorological	Tabular	Input data for model scenarios and model evaluation	Meteorological services
Historical events	Tabular	Reference for model evaluation	Official reports

Unfortunately, no long-term records about debris flows exist in the area. All the volumes specified in Table 3 refer to saturated debris deposits removed shortly after the events.

4 Materials and methods

4.1 Data and parameters

Table 4 summarizes the data and parameters used for the study.

4.1.1 Imagery

Aerial photographs (scale 1:20,000 and 1:60,000) and SPOT satellite imagery (cell size: 2.5 m) were obtained, and digital pictures were taken in all study areas. Orthophotographs were generated from the imagery.

4.1.2 Elevation and relief

High-resolution (5 m) digital elevation models (DEMs) for the study areas were created by stereo-matching of aerial imagery, of digital photographs taken from the opposite slope (Mergili 2007), and of SPOT satellite imagery. The DEMs derived from the different sources were combined in order to make use of the dataset with the best quality for each part of each study area. GPS records in combination with an ASTER DEM were used in places where stereo-matching failed.

4.1.3 Regolith

Samples were extracted from critical areas in gullies, from the sites of shallow slope failures, from steep slopes, and from debris flow deposits.

All samples were extracted from the upper part of the regolith, directly under the frequently occurring shallow cover of coarse gravel. Grain size distribution and the corresponding texture classes were determined for all the samples in a geotechnical laboratory (Fig. 3). Cohesion c (N m^{-2}) and angle of internal friction φ were measured with drained triaxial tests for some of the samples. Hydraulic parameters were derived, using published relationships with texture class (Rawls et al. 1983; Carsel and Parrish 1988): residual water content θ_r and saturated water content θ_s (both in per cent of volume), hydraulic conductivity for the Green–Ampt model K (m s^{-1}), and matric suction at the wetting front ψ (m). Samples with similar properties were aggregated to regolith classes. Class averages of all the parameters were used in the model except for c and φ, where the pairs leading to the most unstable conditions are shown in Table 5. Basic values of the Manning coefficient n_{man} were assigned to each class according to Arcement and Schneider (2000). Due to lacking spatially distributed information on the vertical structure of the regolith in the study areas, one single layer of infinite depth was assumed.

4.1.4 Land cover and surface

The spatial distribution of the land cover classes in the study areas was mapped using aerial images, digital photographs, and field surveys. Characteristic values of interception capacity, rooting depth, vegetation surcharge for n_{man}, and root cohesion were assigned to each class according to values from the literature (Arcement and Schneider 2000; Braud et al. 2001; Schmidt et al. 2001; Bathurst 2002). The published values for most of the parameters scattered over a wide range. n_{man} was determined randomly, constrained by the maxima and minima for each land cover class. For the other values, the averages were applied.

Independently from the land cover classes, two hydrological surface classes HSC were distinguished for each study area, regarding runoff behaviour:

- HSC = 1 includes all cells containing a large, clearly recognizable flow channel. For each cell, the width of this flow channel was defined, based on orthophotographs and field studies;
- HSC = 2 includes cells where slopes are dissected by several small, more or less parallel channels on a sub-cell scale (where runoff concentrates quickly after its initiation), surface runoff occurs as unconcentrated overland flow, or no surface runoff occurs at all. Spatially distributed average channel densities were assigned to the cells of this class and expressed as ratio of the total cell size.

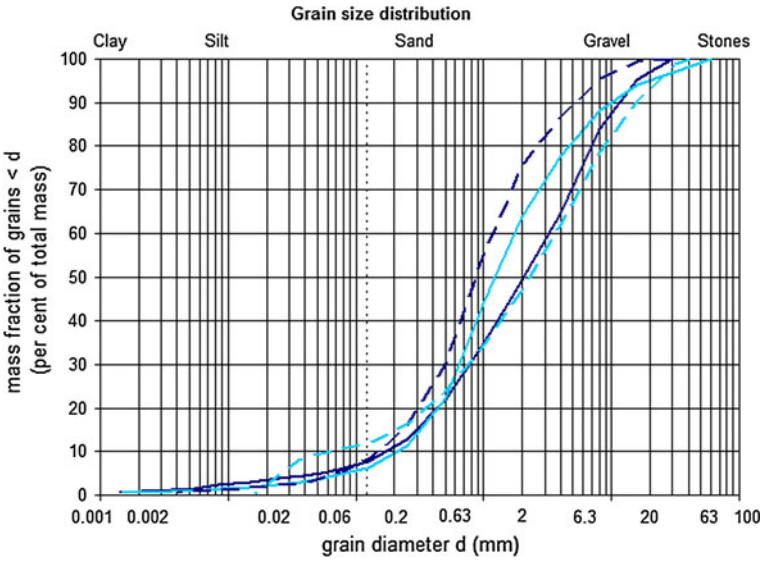

Fig. 3 Grain size distribution of four selected regolith samples collected from the predominantly sandy to gravelly granitic residuals near Guido

Table 5 Regolith parameters for different classes and study areas

Class	*n*	Text class	*c* (kN m^{-2})	φ (deg)	θr (m3 m^{-3})	θs (m3 m^{-3})	ψ (m)	K (m s^{-1})
Granitic residual: *La Ampolleta Quebrada Escondida Castillo de Rocas*	18 (3)	S	0	43.0	0.045	0.43	0.050	3.27E−5
Granitic residual: *Las Murallas*	4 (1)	LS	10	39.5	0.057	0.43	0.061	8.31E−6
Volcanic residual: *Las Murallas*	3 (1)	SL	0	41.3	0.065	0.41	0.110	3.03E−6
Till/talus:*Quebrada del Ferrocarril*	9 (2)	SL	0	40.5	0.065	0.41	0.110	3.03E−6
Till: *Guardia Vieja*	14 (2)	SL	0	38.2	0.065	0.41	0.110	3.03E−6

n = number of samples, in brackets number of samples where c and φ were determined. θ_r and θ_s from Carsel and Parrish (1988); ψ and K from Rawls et al. (1983)

The purpose of the hydrological surface classes and also their definition is closely related to the raster resolution. Let us assume that the model is run with a resolution of 10 m.

First, let us imagine that the terrain forms several small flow channels on sub-cell scale, which—altogether—occupy 20 per cent of the length of each contour line. This would mean that surface runoff would only occur on 20 per cent of the cell, or a width of 2 m. Assuming the water to flow over the entire cell would lead to a misestimation of flow depth and, as a consequence, flow velocity, infiltration, etc. Therefore, a ratio of flow width to cell width is defined (in the above example 0.2), based on field studies and imagery

interpretation, and water is only allowed to flow over the portion of the cell defined by this ratio. Such a raster cell would assume HSC = 2. With unconcentrated overland flow (no recognizable channels), the ratio would be 1.0.

Second, let us imagine a flow channel with a width of 15 m. Again, just working with the cell size would be inappropriate. Such larger flow channels are usually well defined by flow accumulation in the GIS. Therefore, with the presence of such channels, the channel width (in m) is assigned to each cell along the flow path and these cells are assigned HSC = 1, whilst the adjacent cells (which also contain parts of the channel) are HSC = 2. Very wide channels (more than two times the cell size) are also assigned HSC = 2 with a ratio of 1.0.

In summary, the HSC concept helps to reduce the influence of the cell size on the model results. With a very fine spatial resolution (cell size smaller than the width of the narrowest flow channel), the definition of HSC would become obsolete.

4.1.5 Historical data

Published literature (Hauser 2000a) and official reports (Espejo 1996; Hauser 2000b, 2005) were used for model evaluation. They denote efforts and costs for re-establishing transit after debris flows interfering with the international road. These documents include information on the quantities of debris deposited on the road (see Table 3).

4.1.6 Meteorological data

Data on precipitation in the study areas were required for simulating historical or worst-case events. Since no meteorological stations are located in the study areas themselves, the stations Guido and Río Blanco (between 2 and 10 km away from the study areas) had to be used. Precipitation data were available on a daily basis. Breaking down daily precipitation P (mm) into short time intervals was done by assuming different scenarios, based on qualitative information and the known climatic characteristics of the areas. The scenarios were described by duration d_{p} (hours) and maximum intensity i_{p} (mm per hour):

$$i_{\mathrm{p}} = \frac{P}{d_{\mathrm{p}} - d_{\mathrm{p,t}}}, \tag{5}$$

Transition periods $d_{\mathrm{p,t}}$ were assumed at the start and the end of the events.

4.2 The model framework *r.debrisflow*

4.2.1 General model layout

A model framework for the integrated simulation of debris flows triggered by short-duration, high-intensity rainfall events was developed. The tool—named *r.debrisflow*—was designed as a raster module for the Open Source GIS software GRASS, based on the programming language C. It was kept relatively simple in its first version presented here, but was also designed in a way allowing to be extended with more sophisticated modules in the future.

r.debrisflow combines physically based, deterministic model components and components based on empirical-statistical relationships. It couples a hydraulic model, a slope stability model, a sediment transport model, and a model for debris flow motion (Fig. 4).

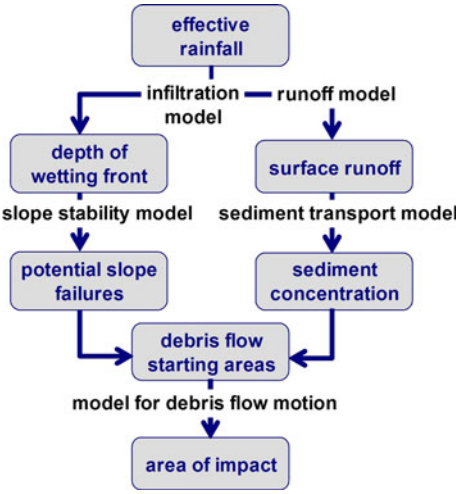

Fig. 4 General model layout of *r.debrisflow*

Simulations are run for a user-defined number of time steps. The slope stability model and the model for debris flow motion, depending on the output of the other components, are run at the end of the last time step.

4.2.2 Hydraulic model components

Rainfall is retained by the vegetation as interception until the interception capacity is reached. The excess rainfall is added to the water table in the regolith as effective rainfall.

Potential evapotranspiration is set to zero as the model is designed primarily for short and intense rainfall events where evapotranspiration is rather negligible.

The Green and Ampt (1911) approach is used for computing infiltration and saturated depth, assuming a wetting front as interface between saturated (above) and unsaturated regolith (below) moving downwards (Fig. 5). Infiltration capacity f (m s^{-1}) is expressed as

$$f = K\left(1 + \frac{R_0 + \psi}{d_0}\right), \tag{6}$$

where d_0 (m) is the depth of the wetting front before infiltration, and R_0 (m) is the flow depth of the surface water before infiltration. K (m s^{-1}) and ψ (m) are parameters estimated from the grain size class (see Table 5). According to Erickson and Stefan (2007), the values of saturated hydraulic conductivity K_s provided by Rawls et al. (1983) are divided by 2 to be applied to the Green–Ampt model in order to account for the unsaturated flow. Equation 6 is derived from Darcy's law. In contrast to some other applications of the Green–Ampt approach, the influence of R_0 on the pressure head is not neglected. If $R_0 > f\,\Delta t$, infiltration is limited by infiltration capacity, and the residual water contributes to surface runoff. The depth of the new wetting front d (m) is computed as

$$d = d_0 + \Delta t \frac{f}{\Delta\theta}, \tag{7}$$

where $\Delta\theta$ (m^3 m^{-3}) is the moisture deficit of the regolith, and Δt is the time step length. The remaining flow depth R (m) follows the relationship

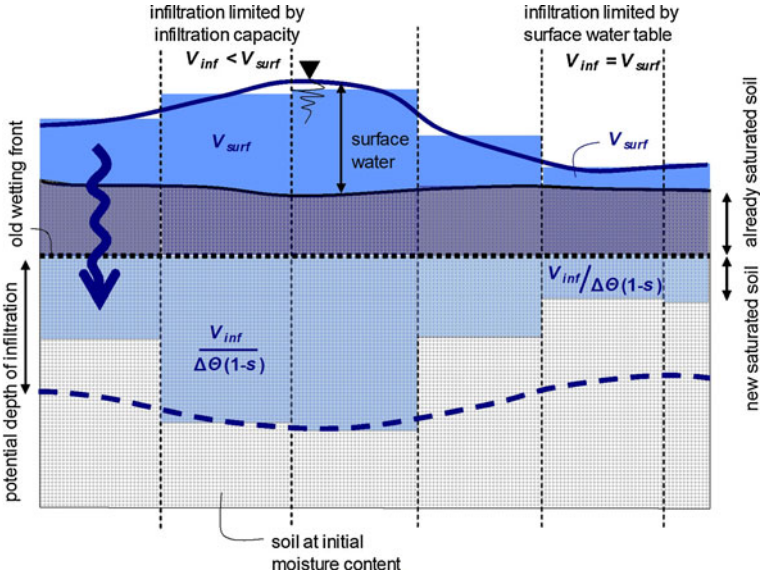

Fig. 5 Infiltration model (modified Green–Ampt approach). V_{surf} = volume of surface water before infiltration, V_{inf} = infiltrated volume

$$R = R_0 - \Delta t \cdot f. \tag{8}$$

If $R_0 \leq f\,\Delta t$, all water infiltrates:

$$d = d_0 + \frac{R_0}{\Delta\theta}, \tag{9}$$

and $R = 0$. The Green–Ampt approach, in a strict sense, was developed for horizontal surfaces, but is also applied for slopes. Chen and Young (2006) showed that on slopes $\leq 45°$, the effect of slope angle is negligible, compared with other sources of inaccuracies. Slope-parallel seepage is neglected in the hydraulic model. For the present study, infiltration is set to zero for bedrock surfaces and all the surface water is considered as surface runoff there. This simplification was required due to the lack of data on the degree of fissuring and related infiltration patterns.

Infiltration is computed separately for regolith below flow channels and in between flow channels. This means that for cells with HSC = 2, two independent infiltration rasters are computed: one applicable for the part where surface runoff occurs (defined by the channel density), and another for the remaining part.

After infiltration, the remaining surface water of the depth R is assumed to concentrate in the flow channels immediately and to run off superficially. Water discharge per unit width q ($m^2\ s^{-1}$) is approximated using Manning's equation:

$$q = v_f R = \frac{1}{n_{man}} R^{\frac{5}{3}} (\sin\alpha)^{\frac{1}{2}}, \tag{10}$$

where v_f ($m\ s^{-1}$) is the runoff velocity, α is the local slope angle in degrees, and n_{man} is the Manning coefficient representing surface roughness. Surface runoff is computed in different ways for the hydrological surface classes:

- HSC = 1 (defined channel): the water is routed through the channel with only one possible downward direction from each cell;
- HSC = 2 (slope with numerous small channels or no channels at all): the water is routed downwards assuming the defined channel densities on a sub-cell scale and a random walk weighted for slope angle.

The length of one time step Δt (s) is defined as

$$\Delta t = a\, d_{\text{cell}}/v_{\max}, \tag{11}$$

where d_{cell} (m) is the cell size and $v_{\max}$ (m s^{-1}) is the maximum flow velocity over the entire area. The constant a is a safety factor ≤ 1 to assure numerical stability (CFL condition). It was set to 0.5. Too short time steps would unnecessarily increase the computing time.

4.2.3 Sediment transport model

If the actual sediment load of surface runoff is below the transport capacity, regolith from the bed is eroded, whilst sediment is deposited in the reverse case. This point of view neglects possible surface armouring, the effects of which are planned to be included in the future development of the model.

Only bedload is considered for the computation of sediment transport and the evolution of debris flows. Runoff is considered to follow (10) below a certain threshold of sediment concentration (see Sect. 4.2.5); at higher sediment concentration it is considered as debris flow.

The Rickenmann (1990) equation is used in the model for estimating sediment transport because it is best suited for relatively steep channels and high sediment concentrations:

$$q_{\text{b}} = \frac{12.6}{(s-1)^{1.6}} \left(\frac{D_{90}}{D_{30}}\right)^{0.2} (q - q_{\text{cr}})(\sin\alpha)^2, \tag{12}$$

where q_{b} (m^2 s^{-1}) is the volumetric bedload transport per unit width, s is the ratio of grain density to fluid density, D_{90} and D_{30} (m) are the grain sizes where 90% and 30% per weight, respectively, are finer, q (m^2 s^{-1}) is the fluid discharge per unit width, and α (degree) is the local slope angle. q_{cr} (m^2 s^{-1}) is the threshold discharge for sediment transport:

$$q_{\text{cr}} = 0.065(s-1)^{1.67} g^{0.5} D_{50}^{1.5} (\sin\alpha)^{-1.12}, \tag{13}$$

where D_{50} (m) is the median grain size, and g (m s^{-2}) is the gravitational acceleration. Erosion (detachment of regolith) or deposition d_{w} (m), depth of bedload l (m), and sediment concentration C (m^3 m^{-3}) are then derived:

$$d_{\text{w}} = \text{ST}(l_0 - q_{\text{b}}/v_l) \quad \text{for } l_0 < q_{\text{b}}/v_{\text{l}}, \tag{14}$$

$$d_{\text{w}} = \text{ST}(l_0 - q_{\text{b}}/v_{\text{l}}) \quad \text{for } l_0 > q_{\text{b}}/v_{\text{l}}, \tag{15}$$

$$l = l_0 - d_{\text{w}} = q_{\text{b}}/v_{\text{l}}, \tag{16}$$

$$C = l/(l+R), \tag{17}$$

where l_0 (m) is the initial depth of bedload and v_{l} (m s^{-1}) is the bedload velocity. The dimensionless calibration parameter ST was introduced for constraining the rate of detachment and deposition (see Sect. 6.3). Negative values of d_{w} (14) indicate detachment, positive values (15) indicate deposition. All the sediment deposited is considered as

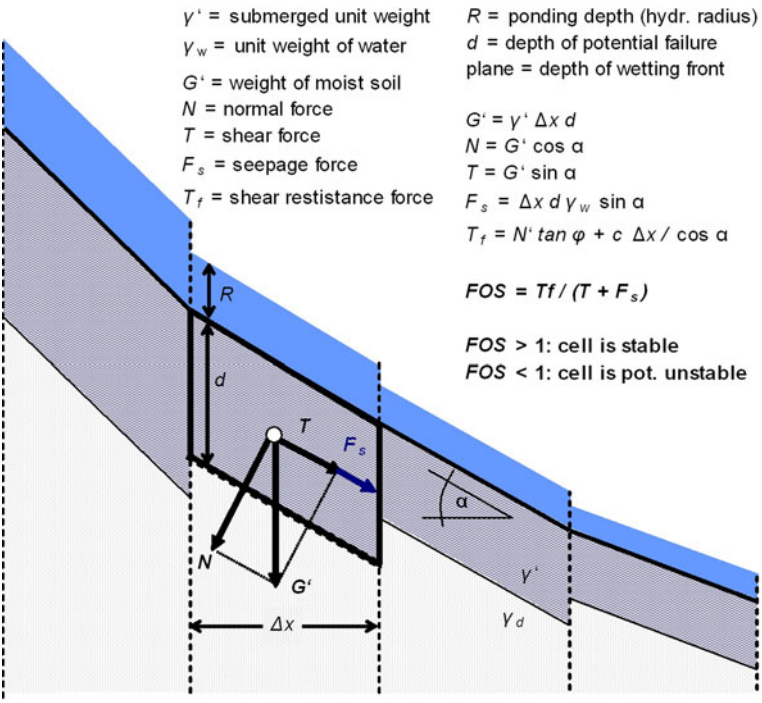

Fig. 6 Slope stability (infinite slope stability model)

saturated, and the depth of the wetting front below the flow channel is corrected for detachment and deposition.

4.2.4 Slope stability model

It is presumed that slope failures only occur at the wetting front. The infinite slope stability model is employed for the calculation (Fig. 6), assuming a slope-parallel flow that exerts a destabilizing seepage force. As discussed above, the infiltration model only includes vertical water flow within the regolith. Assuming slope-parallel flow at the end of the event is therefore a worst-case assumption which is met when the saturated zone is underlain by an impermeable layer (for example bedrock). The dimensionless factor of safety FOS is stated as

$$\mathrm{FOS} = T_\mathrm{f}/(T + F_\mathrm{s}), \tag{18}$$

where T_f is the shear resistance force of the regolith, T is the shear force, and F_s is the seepage force (all in N; see Fig. 6). The shear resistance force is derived from Coulomb's law, and the shear force from a simple mechanical relationship:

$$T_\mathrm{f} = \gamma' \cdot \Delta x \cdot d \cos\alpha \tan\phi + c \cdot \Delta x/\cos\alpha, \tag{19}$$

$$T = \gamma' \cdot \Delta x \cdot d \sin\alpha, \tag{20}$$

where φ is the angle of internal friction, c (N m^{-2}) is the cohesion (cohesion of the regolith c_s plus root cohesion c_r), Δx (m) is the width of the considered slope segment in

downslope direction, and α (degree) is the slope angle. γ' (N m^{-3}) is the specific weight of saturated regolith, including buoyancy:

$$\gamma' = \gamma_d + \gamma_w(\theta_s - 1), \tag{21}$$

where γ_d is the specific weight of dry regolith, γ_w is the specific weight of water (both in N m^{-2}), and θ_s (m^3 m^{-3}) is the saturated volumetric water content. The seepage force exerted by the water in the regolith is stated as

$$F_s = \Delta x \cdot d \cdot \gamma_w \sin\alpha. \tag{22}$$

The forces exerted by the surface water R (m) are neglected in the model. Dry and cohesionless regoliths ($F_s = 0$; $c = 0$; $\gamma' = \gamma_d$) are stable when $\alpha < \varphi$, and unstable when $\alpha > \varphi$.

4.2.5 Debris flow motion and deposition

O'Brien (2003) stated that debris flows are characteristic at a sediment concentration between $C_{min} = 0.45$ and $C_{max} = 0.55$. The lower threshold is well within the range suggested by other authors, whilst much higher values for the upper threshold, up to $C_{max} = 0.90$, were reported (see Coussot and Meunier 1996). Sediment concentration C of surface runoff is therefore tested against C_{min} after each time step. If $C < C_{min}$, the flow continues as surface runoff. If $C \geq C_{min}$, the material is retained from sediment load in order to be routed down as debris flow at the end of the last time step. At the same time, patches of failed regolith are considered as potential source areas of debris flows, too.

Before routing the debris flow downwards, the volume and the area of each of those patches are calculated. If one of these values is below a user-defined threshold, the patch is not further considered. The infinite slope stability model used is only valid as long as the unstable areas are large enough to develop quasi-plain slip surfaces.

The travel distance is computed using a semi-deterministic two-parameter friction model developed by Perla et al. (1980), modified by Gamma (2000) and applied by Wichmann (2006) in a raster-based GIS environment. Since the model is not fully deterministic, a routing algorithm has to be used. It is determined according to the hydrological surface class:

- HSC = 1 (defined channel): the debris flow is routed through the channel with only one possible downward direction from each cell. As soon as deposition occurs within a channel, the corresponding cells are considered as HSC = 2 for the remaining simulation;
- HSC = 2 (no clearly defined channel): a random walk weighted for downslope angle is applied for routing the debris flow.

Each raster cell defined as onset area of debris flows is passed through the routing procedure as individual mass point. The velocity of the debris flow v (m s^{-1}) is computed for each step (i.e. each raster cell the mass point is passed through) i:

$$v_i = \sqrt{\delta_i \left(\frac{M}{D}\right)_i (1 - e^{\beta_i}) + v_{i-1}^2 \, e^{\beta_i} \cos(\Delta\alpha_i)}, \tag{23}$$

where M/D (m) is the mass-to-drag ratio, and v_{i-1} is the debris flow velocity of the previous step. The factor δ_i and the coefficient β_i are derived as follows:

$$\delta_i = g(\sin\alpha_i - \mu\cos\alpha_i), \quad \beta_i = \frac{-2L_i}{(M/D)_i}, \tag{24}$$

where g is the gravitational acceleration (9.81 m s^{-2} on the earth surface), α_i is the local slope angle, μ is the dimensionless friction coefficient, and L (m) is the length of one cell in slope direction. $\Delta\alpha_i$ is the difference between the slope angle of the previous cell and the slope angle of the considered cell, set to zero for convex slopes or channels (Wichmann 2006). For concave slopes, v_{i-1} is corrected as the flow loses energy:

$$v_{i-1} = v_{i-1,0}\cos(\alpha_{i-1} - \alpha_i) \quad \text{if } \alpha_{i-1} > \alpha_i, \tag{25}$$

where the subscript $i - 1$ stands for the previous step (i.e. the previous upslope cell), and 0 for the original value. Values of $M/D = 75$ m were applied, following Wichmann (2006). The following relationship for μ was found to be useful for computing the maximum travel distance (Gamma 2000):

$$\mu = 0.13A^{-0.25}, \tag{26}$$

where A (km^2) is the catchment size for the considered cell. It is assumed that μ would decrease with increasing a because the water content of the debris flow would rise. This relationship was used in *r.debrisflow*. Following Gamma (2000), the range of values of μ would be restricted to a maximum of $\mu_{max} = 0.3$ and a minimum of $\mu_{min} = 0.045$, overruling (26). Wichmann (2006) suggested to set $\mu_{min} = 0.15$.

The two-parameter friction model does not give information on entrainment and deposition. Simple thresholds of slope and velocity are used for delineating these processes in *r.debrisflow*. Entrainment (as far down as to the wetting front) is only assumed if both values are above the thresholds, whilst deposition is assumed to take place only if both values are below. Routing continues until the debris flow has stopped. This happens when the square root in (23) becomes undefined.

4.3 Model scenarios and evaluation

4.3.1 Scenarios

A number of rainfall scenarios was assumed for each study area (except *Quebrada del Ferrocarril*), based on meteorological and historical information (Table 6).

4.3.2 Comparison to observations and reports

Not all the parameters required for running *r.debrisflow* were fully known. This means that the simulation results had to be validated with data on real debris flows. The sediment volumes deposited on the road calculated by the model were compared with the volumes removed from the international road according to official reports (see Table 3). Furthermore, the distribution of starting areas and deposits of debris flows was compared with landslide scars, flow channels, and the maximum extent of debris flow deposits recognizable in the field, on aerial images, and on published photographs.

4.3.3 Analysis of parameter sensitivity

The parameters determining the occurrence or non-occurrence of debris flows are often uncertain, particularly regarding their spatial distribution. A careful analysis of parameter

Table 6 Rainfall scenarios used in the model

Scenario	Rainfall sum (mm)	Met. station	Max. intensity (mm h−1)	Duration (peak + transition) (min)	LA	QE	CR	LM	QF	GV
1	458	Río Blanco	Not defined							x
2	100	Guido	100	40 + 40	x	x	x	x		
3	100	Guido	50	100 + 40	x	x	x	x		
4	40	Guido	80	0 + 40	x	x	x			
5	40	Guido	40	40 + 40	x	x	x	x		
6	40	Guido	20	100 + 40	x	x	x	x		
7	10	Guido	10	40 + 40	x	x	x			
8	Defined starting areas of debris flows								x	

LA *La Ampolleta*, QE *Quebrada Escondida*, CR *Castillo de Rocas*, LM *Las Murallas*, QF *Quebrada del Ferrocarril*, GV *Guardia Vieja*

sensitivity was therefore conducted for assessing the dependency of debris flow occurrence in the study areas on variations of the key parameters: regolith hydraulic properties, calibration parameters for the sediment transport model, regolith and root cohesion c_s and c_r, angle of internal friction φ, influence of drainage direction on slope stability, parameters for modelling the motion of debris flows, and spatial resolution (cell size).

5 Results

A detailed discussion of the model results for all of the study areas and all the rainfall scenarios would go beyond the scope of the present paper. Scenario 2 (100 mm in 80 min; see Table 6) for the study area *Castillo de Rocas* will be presented in detail. Debris flows have repeatedly interfered with the road there in the past and therefore the most reports are available. Furthermore, the model is best applicable to this study area as debris flows start from shallow slope failures and detachment by surface runoff.

The thin black lines in the maps of Figs. 7, 8, 9, 10, 11, 12, 13, 14, 15, 16, 17, and 18 delineate onset and entrainment areas of observed debris flows; the bold black lines indicate observed areas of deposition.

5.1 Infiltration

The infiltration behaviour and the resulting depth of the wetting front are sensitive to a large number of system parameters like pre-wetting of the soil, field capacity, and hydraulic conductivity, all of which are uncertain. Fig. 7 illustrates the depth of the wetting front for different values of the hydraulic conductivity K, ranging from 0.25 K_s to 1.0 K_s for Scenario 2. Increased values of K result in a more rapid infiltration of the surface water and therefore a pronounced increase in the depth of the wetting front beneath the flow channels at the base of bedrock slopes, with a lot of surface water available. Due to the steepness of such areas, an increased potential starting volume of debris flows is the consequence. In contrast, the minimum depth of the wetting front (in between flow channels) is limited by water supply and shows a very low sensitivity to variations of K (Fig. 8). The result with 0.5 K_s was used for the further calculation, following Erickson and Stefan (2007).

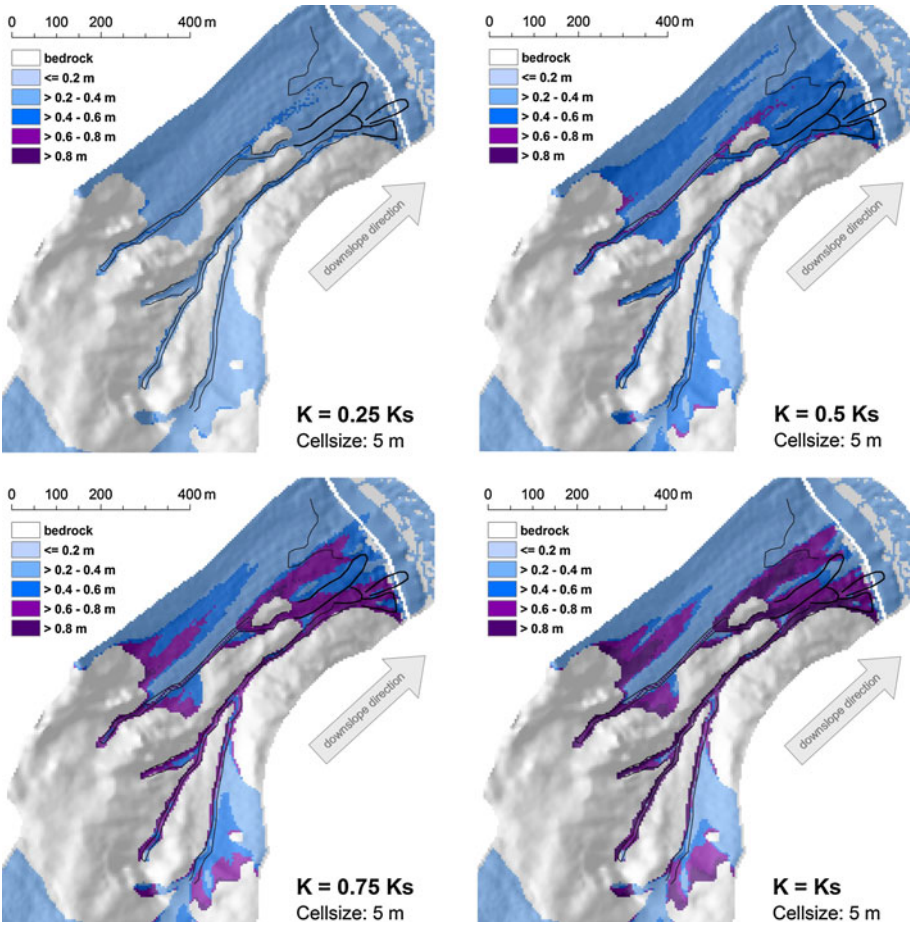

Fig. 7 Depth of the wetting front for Scenario 2 with different values of K

The depth of the wetting front is determined not only by the system parameters and the rainfall sum, but also by rainfall duration. Assuming an event of 100 mm with a duration of 140 min (Scenario 3), the model yielded a deeper wetting front—and therefore a larger volume of regolith prone to instabilities—than for Scenario 2 (Fig. 9).

5.2 Detachment by surface runoff

Since there was no way to compute the velocity of the load v_l in a straightforward way, it was defined by the ratio of flow velocity to load velocity v_f/v_l. Four combinations of v_f/v_l and ST were tested for Scenario 2. As expected, smaller values of v_f/v_l (higher load velocity) lead to a more even distribution of entrainment along the flow path, whilst larger values of v_f/v_l (lower load velocity) result in more pronounced entrainment in the upper portion of the flow path (Fig. 10): with lower load velocities, the potential load depth is larger than with a higher load velocity and the same load discharge, but the flow becomes saturated sooner.

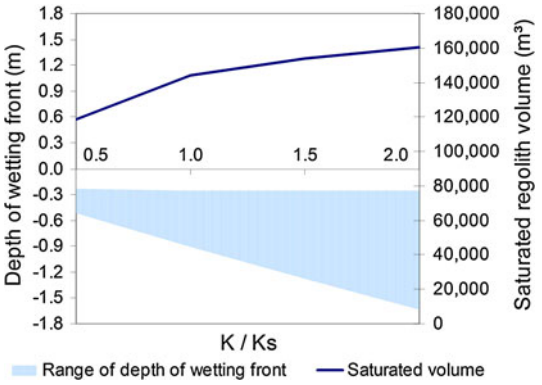

Fig. 8 Sensitivity of the depth of the wetting front and the saturated volume to hydraulic conductivity (same settings as in Fig. 7)

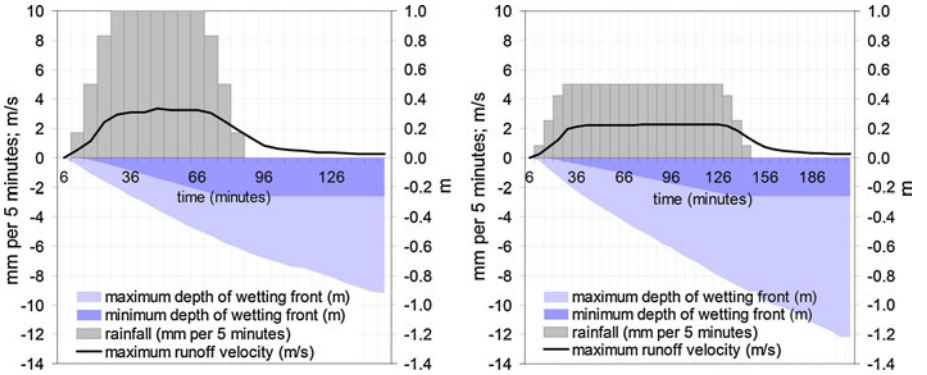

Fig. 9 Modelled temporal development of the depth of the wetting front and velocity of surface runoff for Scenario 2 (*left*) and Scenario 3 (*right*)

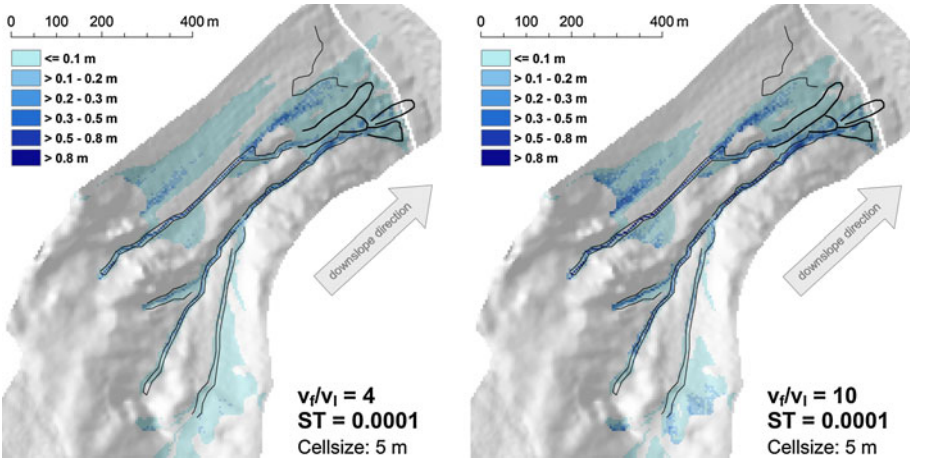

Fig. 10 Simulated depth of detachment by surface runoff (Scenario 2)

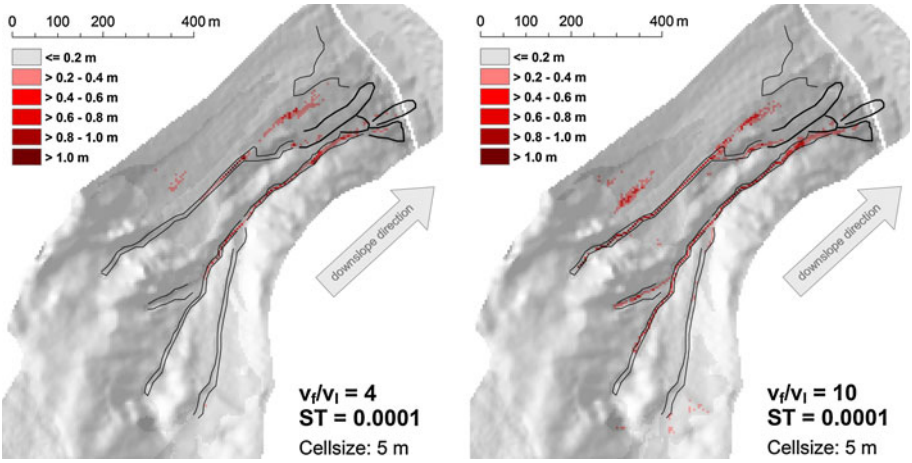

Fig. 11 Simulated depth of onset of debris flows from sediment-laden runoff (Scenario 2)

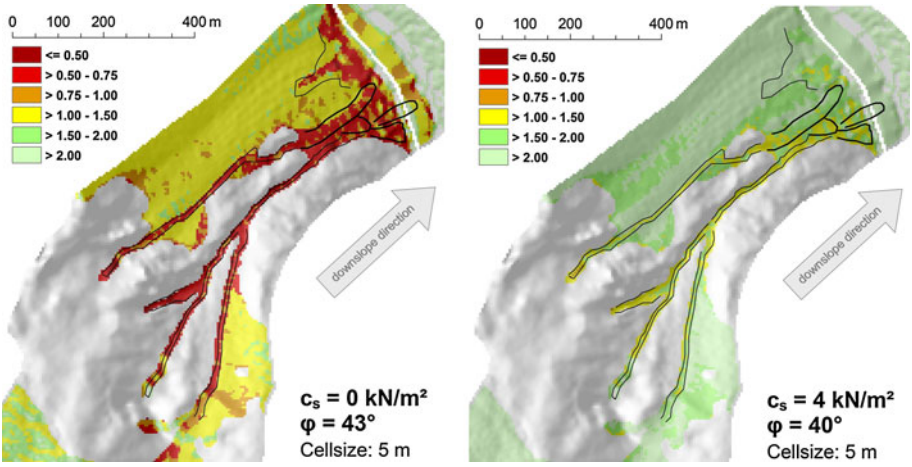

Fig. 12 Factor of safety with different combinations of c_s and φ

Varying the calibration factor for detachment capacity ST also led to the expected outcome: with higher values of ST, the flow soon becomes saturated and much less detachment occurs in the lower portion of the flow channels.

For all four parameter combinations, detachment was predicted predominantly in flow channels and at the base of bedrock outcrops (for the reasons explained above). Observed debris flows onset areas were concentrated particularly in those zones. However, the model results should rather be considered as qualitative information due to the limitations of the Rickenmann (1990) model for such an application and lacking direct reference data (see Sect. 6.3). Most of the major simulated starting areas of debris flows coincided with those identified as mechanically unstable (Fig. 11; see Fig. 13). Therefore, only the latter were considered for debris flow motion since their modelled distribution could be justified in a much better way.

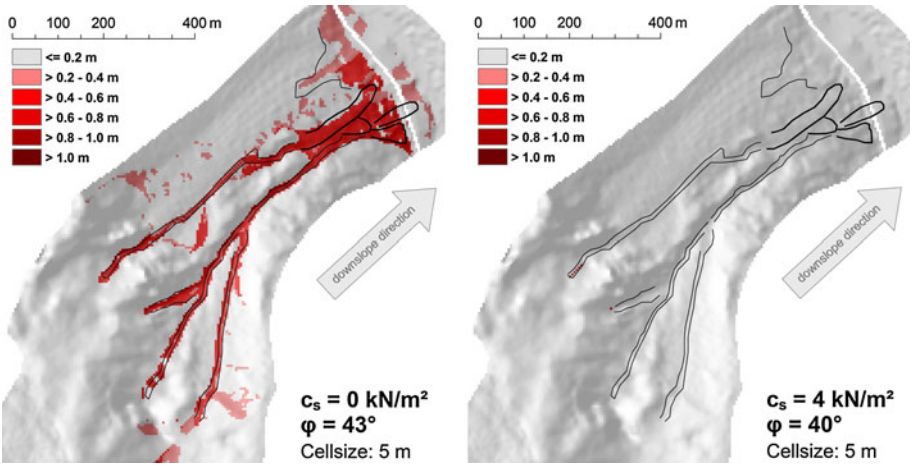

Fig. 13 Depth of potential slope failures with different combinations of c_s and φ

Fig. 14 Dependency of the volume of potential slope failures in the study area Castillo de Rocas on c_s and φ, based on Scenario 2

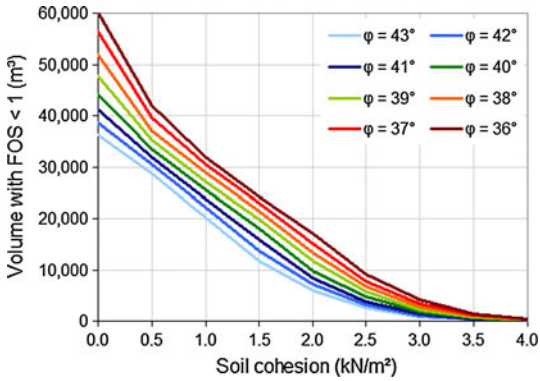

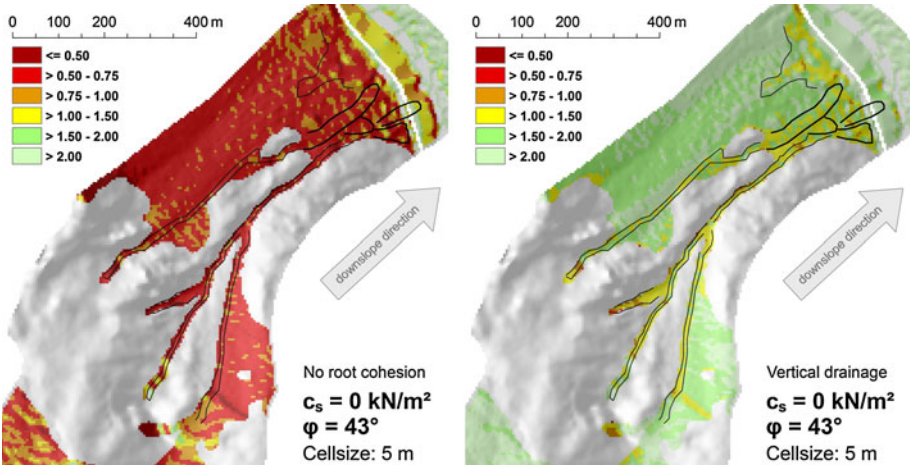

Fig. 15 Factor of safety with disregard of root cohesion (*left*) and with vertical drainage (*right*)

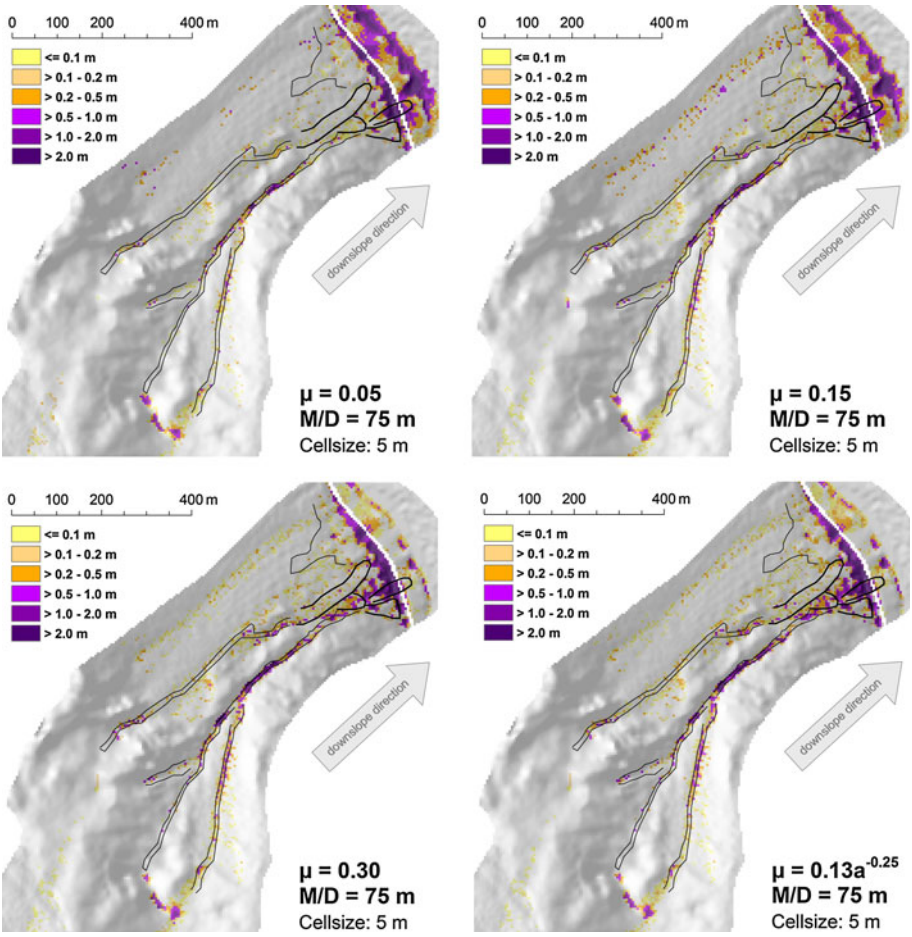

Fig. 16 Simulated depth of debris flow deposits in the study area *Castillo de Rocas*, comparing different values of μ

5.3 Slope stability

The geotechnical analysis of the samples extracted from the granitic regolith in the study area *Castillo de Rocas* yielded values of φ between 36.2° and 43°, and c_s between 0 and 23 kN m^{-2}. As c_s and φ derived from one single triaxial test have to be treated as a pair and not as separate values, the slope stability model was run with each of the four derived pairs, in addition to regularly varying each of the values.

This analysis showed a tremendous sensitivity of the model results particularly to cohesion. As to be expected for shallow instabilities prevailing in the study area, also moderate cohesion values (4 kN m^{-2}) led to a drastic reduction of the potentially unstable areas, compared to non-cohesive regolith, also with lower values of φ (Figs. 12, 13, 14). When applying the pairs $c_s = 10$ kN m^{-2}; $\varphi = 39.5°$ and $c_s = 23$ kN m^{-2}; $\varphi = 36.2°$, no slope failures were simulated at all.

As the unfavourable conditions are of more interest for the present study and as variations of the parameters are rather supposed to be fine-scaled (meaning that unfavourable

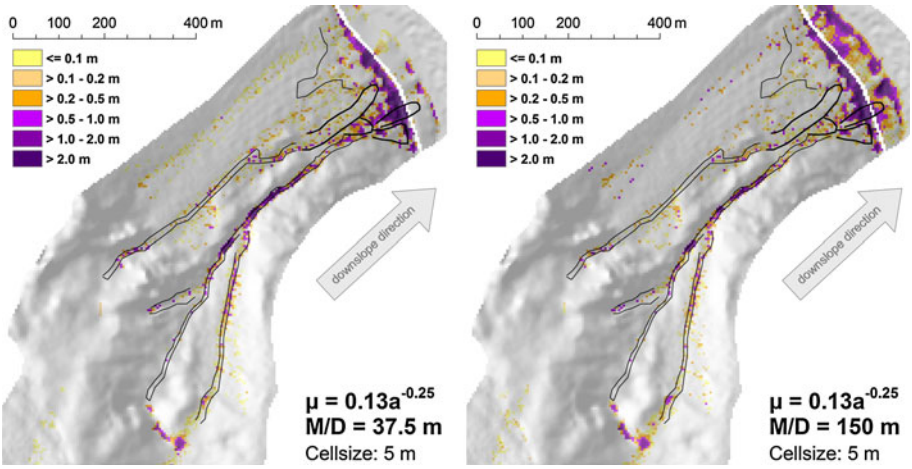

Fig. 17 Simulated depth of deposits with $M/D = 37.5$ (*left*) and $M/D = 150$ (*right*)

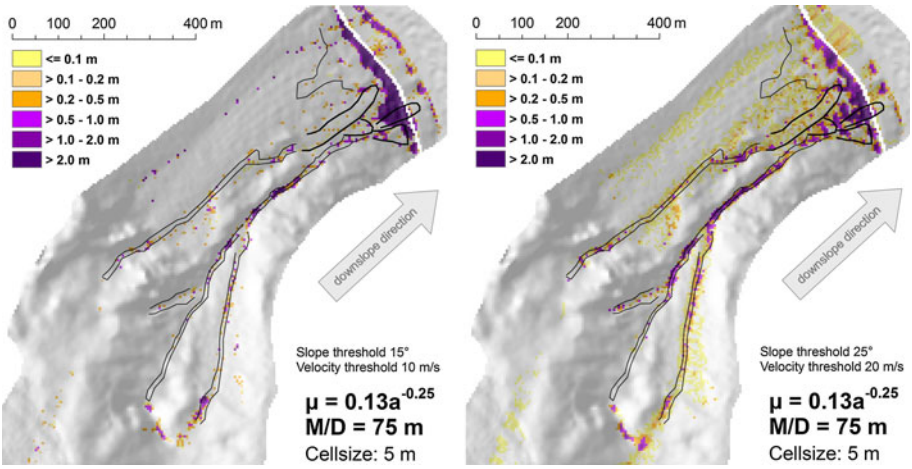

Fig. 18 Simulated depth of deposits with different criteria for entrainment and deposition areas

conditions occur in each small patch of slope and govern its stability), the pair with $c_s = 0$ kN m^{-2} and $\varphi = 43°$ was further applied in the model. Areas with FOS < 1 are mainly concentrated in steep channels and directly upslope from the road, corresponding well to field observations (see Figs. 12, 13).

For the cohesionless regolith in the study area, the depth of the wetting front does only influence depth, but not the spatial distribution of potentially unstable areas unless another regolith layer comes into action or rooting depth is exceeded.

Two further tests of parameter sensitivity for slope stability were conducted (Fig. 15):

- Omitting root cohesion had a significant effect on slope stability—almost the entire regolith slopes were identified as unstable. Vegetation obviously inhibits the onset of debris flow processes, but on the other hand also establishes better in undisturbed areas;

- The direction of water movement in the regolith turned out to be important, too: with vertical drainage, the slopes are much more stable than with the standard slope-parallel water movement in the regolith.

5.4 Debris flow motion

Various combinations of μ, M/D, and slope and velocity thresholds for entrainment and deposition were tested in order to determine the set of parameters reproducing the observed patterns in the best way.

The lower part of the study area *Castillo de Rocas* is crossed by a road, characterized by a very small slope angle, whilst the slopes directly upwards show slope angles up to 30° or more. Downslope from the road, the slope is steep again down to the valley bottom. These characteristics clearly govern the patterns of debris flow deposition suggested by the simulation: except for some patches in the flow channels, two clearly defined domains of deposition are visible—one of them on or directly adjacent to the road, the other one where the slope merges with the valley bottom. The relative importance of the two deposits shifts depending on the combination of parameters used (Figs. 16, 17, 18). In reality, most of the material from past debris flows was deposited on or directly adjacent to the road. With increasing μ, the simulated debris flow volume deposited on the road steadily decreases from 4,490 m^3 ($\mu = 0.05$) to 2,800 m^3 ($\mu = 0.3$): with higher bed friction, more material would already be deposited farther upslope.

The best fit with the observed travel distance of most of the material was found with the parameters μ and M/D proposed by Wichmann (2006), with μ as a function of the catchment area (see Eq. 26), and with thresholds of 20° (slope) and 15 m s^{-1} (velocity) for entrainment and deposition. With these parameters, 2,760 m^3 of debris were predicted to deposit on the road. Assuming $M/D = 37.5$ yielded a value of 2,240 m^3, doubling M/D to 150 yielded 4,380 m^3. A sensitive response was also observed when varying the slope and velocity thresholds for entrainment and deposition. With 25° and 20 m s^{-1}, much of the material was deposited farther upslope and only 1,530 m^3 on the road, whilst with 15° and 10 m s^{-1}, 6,750 m^3 of debris were deposited on the road, according to the simulation.

It turned out hard to reproduce the observed patterns of deposition in a satisfactory way:

- part of the deposits was removed directly after the event in order to re-establish traffic on the road, so that the reference data are incomplete;
- this type of model does not represent the process in a fully deterministic manner, so that it is only possible to reproduce one single parameter of interest, e.g. travel distance, rather than to fit the simulation to all observed debris flow characteristics. This aspect is also the reason for the fact that the modelled velocities were rather too high, exceeding 20 m s^{-1}.

5.5 Sensitivity of the model to cell size

Within the range of 5–10 m, the infiltration model, the surface runoff model, and the slope stability model are not very sensitive to variations of cell size (Fig. 19; Table 7). Also with 20 m cell size, the key output parameters remain within the same magnitude, supporting the applied concept of hydrological surface classes.

The sediment transport model reacts sensitive to a change from 5 to 10 m cell size: errors caused by moderate topographic smoothing multiply by numerous feedback effects.

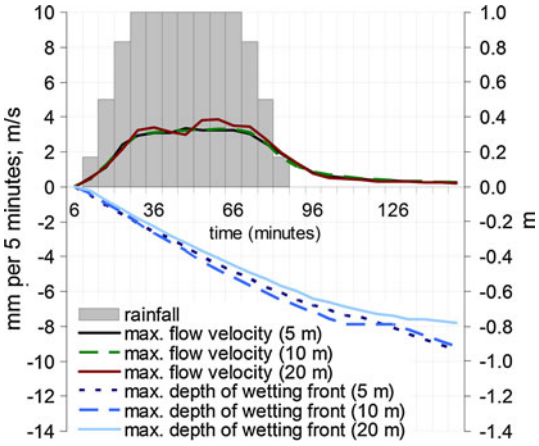

Fig. 19 Sensitivity of the depth of the wetting front and the maximum velocity of surface runoff to variations in cell size (5, 10, and 20 m)

Table 7 Sensitivity of selected output parameters to cell size

Cell size (m)	v_{max} (m s^{-1})		d_{max} (m)		V_{det} (m^3)		V_{fp} (m^3)		V_{dr} (m^3)	
5	3.33		0.94		9,561		37,881		2,849	
10	3.31	−0.6%	0.92	−2.1%	7,024	−26.5%	38,050	0.4%	2,020	−29.1%
20	3.85	15.6%	0.78	−17.0%	4,295	−55.1%	33,206	−12.3%	1,078	−62.2%

v_{max} = maximum velocity of surface runoff, d_{max} = maximum depth of the wetting front, V_{det} = volume of regolith detached by surface runoff, V_{fp} = volume of regolith with FOS < 1, V_{dr} = debris flow volume deposited on the road. The percentages denote the changes compared to the results computed with a cell size of 5 m.

Whilst the debris flow motion model in general turned out to be relatively robust against changes of cell size, the predicted deposit on the road is highly sensitive. This is mainly due to the limited width of the road, which is not properly represented when applying a cell size of 10 or 20 m.

According to Wichmann (2006), the applied type of debris flow motion model is not very sensitive to cell size until 25 m. A further reduction of spatial resolution is supposed to smooth out important topographic features, negatively affecting the quality of the results of all model components.

5.6 Comparison with reports and field observations

Table 8 provides a comparison of the modelled debris flow starting volumes and deposits to the reference volumes. In all cases, simulated and reported values correspond in their order of magnitude. However, it was not possible to confirm an increase of debris flow volume with increasing rainfall. For the Guido area, a 600 m^3 deposit on the road was reported for a 40 mm rainfall event, whilst 15,000 m^3 were reported for a 9.2 mm rainfall event a few weeks earlier (Espejo 1996). This may reflect the small-scale patterns of precipitation in and around the study areas as well as the influence of available unstable material (much may have been removed during the first event). However, it also illustrates the virtual impossibility to perform spatio-temporal predictions with this type of model. Much more, approaching worst-case scenarios is a realistic goal.

Table 8 Ranges of volumes included in debris flows according to the different scenarios for all the study areas used

Study area	Modelled starting volume (m^3)	Estimated starting volume (m^3)	Modelled deposit on road (m^3)	Reported volume on road (m^3)	Remarks
La Ampolleta	7,200–70.400	7,000–15,000	300–4,300	600–15,000	Reports include some material from rock fall; no more differentiated data available
Quebrada Escondida	2,000–13,200	3,000–6,000	300–2,500		
Castillo de Rocas	5.800–57,200	7,000–35,000	200–4,400		
Las Murallas	22,100–37,900	10,000–50,000	700–1,700		
Quebrada del Ferrocarril	36,000	20,000–75,000	9,800	8,000–14,000	Defined starting volume (snow melt-triggered debris flows)
Guardia Vieja	1,969,000	>140,000	100,000	45,000	Infiltration of entire effective rainfall assumed

For the study area *Guardia Vieja*, the spatial patterns of slope failure were not predicted in a satisfactory way. This is not surprising because the instabilities there were rather deep-seated rotational, caused by longer rainfall events (several hours to days), so that neither the Green–Ampt approach nor the infinite slope stability model were well applicable. For *Quebrada del Ferrocarril*, only debris flow motion was computed with defined starting areas since debris flows there were predominantly triggered by rapid snow melt and specific circumstances (Hauser 2000b). Most of the debris flows in the study area *Quebrada del Ferrocarril* were simulated to cease close to their starting areas when using $\mu_{\min} = 0.15$ according to Wichmann (2006). When following Gamma (2000) and setting $\mu_{\min} = 0.045$, as well as reducing the slope threshold for entrainment and deposition, the model results corresponded much better to the reference information. This may indicate a higher water content of the flows.

Also for the remaining study areas, μ as well as the thresholds for entrainment and deposition had to be calibrated in order to match the simulated travel distance with the field observations. Table 9 illustrates the values applied.

6 Discussion

6.1 General aspects

In general, the observations and historical records for the study areas were reconstructed well by the model, the limitations are discussed below. The prediction of the response to specific rainfall events and the derivation of rainfall thresholds are particularly problematic due to the model used for water flow in the regolith (saturation of

Table 9 Parameter settings found to be suitable for the study areas

Study area	M/D (m)	μ	μ_{min}	μ_{max}	Slope threshold (°)	Velocity threshold (m s^{-1})
La Ampolleta	75	0.25	–	–	15	10
Quebrada Escondida	75	0.25	–	–	15	10
Castillo de Rocas	75	$0.13a^{-0.25}$	0.15	0.3	20 (27.5)	15 (17.5)
Las Murallas	75	$0.13a^{-0.25}$	0.045	0.3	20	15
Quebrada del Ferrocarril	75	0.045	–	–	8	10
Guardia Vieja	75	0.1	–	–	15	10

the uppermost regolith layer also with minor rainfall events) and, specifically for the study areas used, lacking correlation between magnitude of reported events and corresponding rainfall data. The suitability of the model—and of this type of models in general—for Class A predictions (such predictions made before the event without model calibration by direct reference data, Lambe 1973) turned out to be very limited. Specific issues related to each model component and possible solutions are briefly discussed below.

6.2 Infiltration model

Water movement in the regolith was modelled in a plausible way without calibration, but the possibilities for direct validation were limited. Unsurprisingly, the infiltration model reacts highly sensitively to the soil hydraulic parameters. Soil hydraulic conductivity K is of particular interest as significantly different values appear in the literature for one and the same class of regolith (Rawls et al. 1983; Carsel and Parrish 1988) and there is disagreement whether to use saturated hydraulic conductivity K_s or not (Xie et al. 2004; Erickson and Stefan 2007) when employing the Green–Ampt model. Furthermore, the spatial distribution of soil classes is often fine-scaled, but—as in the present study—lumped values have to be used for entire slopes due to lacking information at a higher level of detail. Considering all these problems, it is possible only to provide a range of realistic depths of the wetting front.

The response of the model to variations of K is not linear. With higher hydraulic conductivity, surface water flow moving from upslope bedrock onto the regolith-covered slope infiltrates faster, so that the flow does not reach as far down as with lower values of K. Therefore, areas with deeper wetting front despite lower K exist at some distance downslope or downstream of rock outcrops (see Fig. 7).

The hydraulic status of the soil at the beginning of the triggering event is an additional source of uncertainty: pre-wetting significantly changes the infiltration and runoff behaviour.

6.3 Sediment transport model

It turned out that the straightforward implementation of an adequate sediment transport algorithm was not possible. The Rickenmann (1990) approach appears best suitable for the

conditions in the study areas (Hessel and Jetten 2007), but its usefulness in a dynamic model is limited by the following serious problems:

- the velocity of the bedload transport does not equal the velocity of the water flow. This fact does not matter when only the bedload transport capacity is considered, but it does when routing the bedload downstream and dynamically computing potential detachment and deposition on a pixel base. The ratio of water velocity to bedload velocity is hardly known.
- the approach does not provide any information on possible rates of detachment and deposition, only about a dynamic equilibrium. This complex of problems could be attacked by combining the Rickenmann algorithm with detachment algorithms (see Sect. 2.2.2 for references), but a careful calibration of the parameters with real data would be needed.

Furthermore, the approach was developed and calibrated for channels $\leq 20°$ and reacts very sensitive to variations of the slope (Hessel and Jetten 2007), so that more experimental work would be required to make it better applicable to the catchments used in the present study. The disregard of suspended load may lead to additional inaccuracies.

6.4 Slope stability model

In general, domains with lower computed values of FOS corresponded well to areas where onset areas of debris flows were observed. The limiting factor for the success of such simulations, however, is the lack of knowledge on the spatial distribution of the parameters governing slope stability. The results of the geotechnical analyses performed in the present study illustrate the huge variation of the parameters even in areas with rather homogeneous regolith. However, under such conditions, the variations are rather supposed to occur in a small-scale pattern. Therefore, it appears acceptable to use the most unfavourable set of values for deriving worst-case scenarios. However, a better understanding of the spatial distribution of the key parameters—including the vertical structure of the regolith (depth, impermeable layers, pre-wetting, etc.)—would be required for reducing the uncertainties. In addition, high-resolution imagery and DEM information from directly before and after the event would be extremely helpful to better constrain starting areas and involved volumes.

The model turned out unsuccessful in areas with prevailing rotational slope failures, particularly in the study area *Guardia Vieja*. Algorithms required to model rotational failures differ substantially from the infinite slope stability concept. Several models are applied by geotechnicians (e.g. Schneider-Muntau and Fellin 2005), but GIS-based approaches are rare due to the non-trivial implementation of appropriate algorithms and iteration procedures as well as due to the problems with 3D processes in 2D raster systems. Xie et al. (2003, 2006) criticized the concentration on the infinite slope stability concept in slope stability modelling and introduced a GIS-based model for rotational failures. Mergili and Fellin (2009) implemented a model for rotational failures based on GRASS GIS which shall be included in *r.debrisflow* in the future.

Another source of uncertainty is the issue of process interactions. In many cases it is not trivial to decide whether a debris flow did actually start from slope failure (FOS < 1) or from detachment—in some of the study areas presented, there is good reason to assume that both processes were involved, i.e. by the interaction of powerful surface runoff with slopes on the verge of failure (FOS ≈ 1). More research is needed in order to better understand such interactions.

6.5 Debris flow motion and deposition

For the study area *Castillo de Rocas*, the travel distance, but not the shape of the deposit of past debris flows, was successfully simulated using the parameters M/D and μ suggested by Wichmann (2006). For the other study areas, μ had to be calibrated in order to bring the computed travel distances in line with the observations (see Table 9). Simulating the areas of entrainment and deposition in a realistic way required an even higher degree of calibration and failed for the study area *Castillo de Rocas* (see Sect. 5.4 for an explanation). This means that such model approaches have only a very limited suitability for Class A predictions. A comprehensive set of parameter values suitable for different types of debris flows over different topographies and with different volumes would be needed, requiring extensive field observations.

A further problem of those semi-deterministic approaches is that they actually consider mass points, disregarding the volume of the entire flow. Increased volumes can only be accounted for indirectly by increasing M/D.

Future work shall be directed towards an improved parameterization on the one hand, and the inclusion of a physically based model on the other hand. The latter shall also be able to predict entrainment as well as energies and impact forces. Mergili et al. (2008) have produced a prototype of a GRASS GIS implementation of the Savage and Hutter (1989) model for simple topographies.

6.6 Conclusions

The present paper deals with the simulation of debris flows on the small catchment scale. Different techniques for modelling a variety of relevant processes were combined in a model framework realized in GRASS GIS. The goal was to reconstruct past debris flows in selected small catchments and to evaluate the potentials and limitations of the model components. GRASS GIS appeared highly suitable for this task as its modular structure allows for the implementation of complex algorithms due to the support of the C programming language.

Modelling of processes related to the onset of debris flows (particularly infiltration and slope failure) is rather limited by the available data. Despite extensive field visits, sampling, and laboratory analyses, considerable uncertainties with the governing parameters and—in particular—their spatial distribution became apparent. The modelling techniques existing for such processes appear appropriate in general, but are sensitive to the uncertain data. Systematic approaches for tackling uncertainties exist (Bathurst et al. 2004, 2005), e.g. the GLUE (General Likelihood Uncertainty Estimation) approach proposed by Beven and Binley (1992) or blind validation (Ewen and Parkin 1996). However, their application would require more reference data, particularly on the system-internal parameters (e.g. water status of the slope).

Simulation of dynamic processes like sediment transport, the propagation of debris flows, or entrainment, or of process interactions, is also limited by the available modelling techniques. Simple approaches are not suitable for Class A predictions and often require complex parameters hard to determine. The present study has shown that the travel distance may be well estimated using semi-deterministic approaches, whilst fully deterministic models would be required for deriving also velocities and impact energies. The choice of the appropriate model therefore strongly depends on the desired information.

Acknowledgments The study was funded by the Tyrolean Science Funds, the University of Innsbruck, and the Government of Upper Austria. Special thanks go to J. Espejo and A. Hauser for making available substantial reference data.

References

Abrahams AD, Li G, Krishnan C, Atkinson JF (2001) A sediment transport equation for interrill overland flow on rough surfaces. Earth Surf Process Landf 26:1443–1459

Arcement GJ, Schneider VR (2000) Guide for selecting Manning's roughness coefficients for natural channels and flood plains. USGS Water-supply Paper 2339

Bagnold RA (1980) An empirical correlation of bedload transport rates in flumes and natural rivers. Proc R Soc Lond Ser A. Containing Papers of a Mathematical and Physical Character 372

Bathurst J (2002) DAMOCLES. Debrisfall assessment in mountain catchments for local end-users. Detailed Report of Contractor for Fifth Progress Meeting. University of Newcastle upon Tyne, UK. http://damocles.irpi.cnr.it/docs/November-2002/Newcastle-November2002.pdf

Bathurst JC, Ewen J, Parkin G, O'Connell PE, Cooper JD (2004) Validation of catchment models for predicting land-use and climate change impacts. 3. Blind validation for internal and outlet responses. J Hydrol 287:74–94

Bathurst JC, Moretti G, El-Hames A, Moaven-Hashemi A, Burton A (2005) Scenario modelling of basin-scale, shallow landslide sediment yield, Valsassina, Italian Southern Alps. Nat Hazards Earth Syst Sci 5:189–202

Beven K, Binley A (1992) The future of distributed models: model calibration and uncertainty prediction. Hydrol Process 6:279–298

Braud I, Vich AIJ, Zuluaga J, Fornero L, Pedrani A (2001) Vegetation influence on runoff and sediment yield in the Andes region: observation and modelling. J Hydrol 254:124–144

Burton A, Bathurst JC (1998) Physically based modelling of shallow landslide sediment yield at a catchment scale. Environ Geol 35:89–99

Carsel RF, Parrish RS (1988) Developing joint probability distributions of soil water retention characteristics. Water Resour Res 24:755–769

Chau KT, Lo KH (2004) Hazard assessment of debris flows for Leung King Estate of Hong Kong by incorporating GIS with numerical simulations. Nat Hazards Earth Syst Sci 4:103–116

Chen L, Young MH (2006) Green–Ampt infiltration model for sloping surfaces. Water Resour Res 42:W07420. doi:10.1029/2005WR004468

Corominas J, Copons R, Vilaplana JM, Altamir J, Amigó J (2003) Integrated landslide susceptibility analysis and hazard assessment in the principality of Andorra. Nat Hazards 30:421–435

Coussot P, Meunier M (1996) Recognition, classification and mechanical description of debris flows. Earth Sci Rev 40:209–227

Erickson T, Stefan HG (2007) Groundwater recharge from a changing landscape. Project Report No. 490, St. Anthony Falls Laboratory, University of Minnesota

Espejo J (1996) Unpublished reports about mass movements interfering with the international road from Mendoza to Central Chile (in Spanish)

Ewen J, Parkin G (1996) Validation of catchment models for predicting land-use and climate change impacts. 1. Method. J Hydrol 175:583–594

Gamma P (2000) dfwalk—Ein Murgang-Simulationsprogramm zur Gefahrenzonierung. Geographica Bernensia G66 (in German)

Govers G (1990) Empirical relationships for transport capacity of overland flow. IAHS Publ 189:45–63

Green WH, Ampt GA (1911) Studies on soil physics. J Agric Sci 4:1–24

Hauser A (2000a) Remociones en masa en Chile (versión actualizada). Servicio Nacional de Geología y Minería, Subdirección Nacional de Geología, Boletín No. 59, Santiago de Chile (in Spanish)

Hauser A (2000b) Flujos detríticos en segmento del Camino Internacional a Argentina, sector Juncal—Paso Los Libertadores: Causas, efectos, medidas de control. Report of the Servicio Nacional de Geología y Minería, Subdirección Nacional de Geología, Santiago de Chile (in Spanish)

Hauser A (2005) Evaluación de vulnerabilidad y propuesta de procedimientos para el control de flujos detríticos o aluvionales en segmento Juncal-Portillo, del Camino Internacional a la República

Argentina. Report of the Servicio Nacional de Geología y Minería, Subdirección Nacional de Geología, Santiago de Chile (in Spanish)
Hessel R, Jetten V (2007) Suitability of transport equations in modelling soil erosion for a small Loess Plateau catchment. Eng Geol 91:56–71
Hungr O (1995) A model for the runout analysis of rapid flow slides, debris flows, and avalanches. Can Geotechnol J 32:610–623
Iverson RM (1997) The physics of debris flows. Rev Geophys 35:245–296
Jarvis A, Reuter HI, Nelson A, Guevara E (2008) Hole-filled seamless SRTM data V4. International Centre for Tropical Agriculture (CIAT), available from http://www.srtm.csi.cgiar.org
Knapen A, Poesen J, Govers C, Gyssels G, Nachtergaele J (2007) Resistance of soils to concentrated flow erosion: a review. Earth Sci Rev 80:75–109
Lambe TW (1973) Predictions in soil engineering. Géotechnique 23(2):149–202
Low HS (1989) Effect of sediment density on bedload transport. J Hydraul Eng 115:124–138
Mergili M (2007) Stereo matching of terrestrial digital photographs—an alternative for the generation of high-resolution DEMs in situations of poor data availability? In: Car A, Griesebner G, Strobl J (eds) Geospatial crossroads @ GI_Forum—Proceedings of the 1st Geoinformatics Forum Salzburg, pp 110–119
Mergili M, Fellin W (2009) Slope stability and geographic information systems: an advanced model versus the infinite slope stability approach. In: Proceedings of the international conference "mitigation of natural hazards and risks—georisk 2009", Moscow, 21 May 2009, pp 119–124
Mergili M, Schratz K, Thalhammer M, Fellin W, Ostermann A (2008) An open source model for the simulation of granular flows: first results with GRASS GIS and needs for further research. In: Academic Proceedings of the 2008 free and open source software for geospatial (FOSS4G) conference, 29 Sept–3 Oct, Cape Town, pp 231–238
Moreiras SM (2004a) Landslide incidence zonation in the Rio Mendoza Valley, Mendoza Province, Argentina. Earth Surf Process Landf 29:255–266
Moreiras SM (2004b) Landslide susceptibility zonation in the Rio Mendoza Valley, Argentina. Geomorphology 66:345–357
Moreiras SM (2005) Climatic effect of ENSO associated with landslide occurrence in the Central Andes, Mendoza Province, Argentina. Landslides 2:53–59
O'Brien JS (2003) FLO-2D users' manual version 2003.06, July 2003. FLO-2D Software Inc., Nutrioso
Pack RT, Tarboton DG, Goodwin CN (1998) The SINMAP approach to terrain stability mapping. Paper Submitted to 8th Congress of the International Association of Engineering Geology, Vancouver
Perla R, Cheng TT, McClung DM (1980) A two-parameter model of snow avalanche motion. J Glaciol 26:197–207
Rawls WJ, Brakensiek DL, Miller N (1983) Green–Ampt infiltration parameters from soil data. J of Hydr Eng 109:62–70
Rickenmann D (1990) Bedload transport capacity of slurry flows at steep slopes. Mitteilungen der Versuchsanstalt für Wasserbau, Hydrologie und Glaziologie, ETH Zürich 103
Rickenmann D (1999) Empirical relationships for debris flows. Nat Hazards 19:47–77
Savage SB, Hutter K (1989) The motion of a finite mass of granular material down a rough incline. J Fluid Mech 199:177–215
Schmidt KM, Roering JJ, Stock JD, Dietrich WE, Montgomery DR, Schaub T (2001) The variability of root cohesion as an influence on shallow landslide susceptibility in the Oregon Coast Range. Can Geotechnol J 38:995–1024
Schneider-Muntau B, Fellin W (2005) Fallstudie Mure Nals—Untersuchung des Muranbruchs mittels Standsicherheitsberechnung. Österreichische Ingenieur- und Architektenzeitschrift 150:42–45 (in German)
Schoklitsch A (1962) Handbuch des Wasserbaues, 3rd edn. Springer, Vienna (in German)
Takahashi T, Nakagawa H, Harada T, Yamashiki Y (1992) Routing debris flows with particle segregation. J Hydrol Res 118:1490–1507
Vandre BC (1985) Rudd Creek debris flow. In: Bowles DS (ed) Delineation of landslide, flashflood, and debris flow hazards in Utah. Utah Water Research Laboratory, Utah State University, Logan
Wichmann V (2006) Modellierung geomorphologischer Prozesse in einem alpinen Einzugsgebiet. Abgrenzung und Klassifizierung der Wirkungsräume von Sturzprozessen und Muren mit einem GIS. Eichstätter Geographische Arbeiten 15 (in German)
Wilkinson PL, Anderson MG, Lloyd DM (2002) An integrated hydrological model for rain-induced landslide prediction. Earth Surf Process Landf 27:1285–1297
Xie M, Esaki T, Zhou G, Mitani Y (2003) Three-dimensional stability evaluation of landslides and a sliding process simulation using a new geographic information systems component. Environ Geol 43:503–512

Xie M, Esaki T, Cai M (2004) A time-space based approach for mapping rainfall-induced shallow landslide hazard. Environ Geol 46:840–850

Xie M, Esaki T, Qiu C, Wang C (2006) Geographical information system-based computational implementation and application of spatial three-dimensional slope stability analysis. Comput Geotech 33:260–274

Yalin MS (1963) An expression for bedload transportation. J Hydraul Div Proc Am Soc Civ Eng 89:221–250

Yang CT (1973) Incipient motion and sediment transport. J Hydraul Div Proc Am Soc Civ Eng 99:1679–1703